



HAL
open science

Temperature Anomalies and Carbon Dioxide, a Correlation Attempt

Michel de Rougemont

► **To cite this version:**

Michel de Rougemont. Temperature Anomalies and Carbon Dioxide, a Correlation Attempt. 2015, pp.19. hal-01146608v1

HAL Id: hal-01146608

<https://hal.science/hal-01146608v1>

Submitted on 28 Apr 2015 (v1), last revised 14 Jul 2015 (v3)

HAL is a multi-disciplinary open access archive for the deposit and dissemination of scientific research documents, whether they are published or not. The documents may come from teaching and research institutions in France or abroad, or from public or private research centers.

L'archive ouverte pluridisciplinaire **HAL**, est destinée au dépôt et à la diffusion de documents scientifiques de niveau recherche, publiés ou non, émanant des établissements d'enseignement et de recherche français ou étrangers, des laboratoires publics ou privés.

Temperature Anomalies and Carbon Dioxide, a Correlation Attempt

Michel de Rougemont¹

Warming of the global climate is usually correlated with atmospheric carbon dioxide (CO₂) concentration. The sensitivity of global surface temperature to rising CO₂ concentration was evaluated over the period 1853 to present. Publicly available datasets were used including temperature anomalies, CO₂ concentration, global sea level, oceanic oscillations, solar activity, and magnetic field declination. A specific, statistically significant contribution to global warming of the CO₂ atmospheric concentration could not be extracted from the available dataset. While comparing the calculation results from a simple radiative forcing and feedback model with the observed global warming, the CO₂ contribution is estimated to be less than 25 to 30% of the total, while other causes contribute for the rest. Thus, the “Equilibrium Climate Sensitivity” is estimated to be at 0.53°C (0.42 to 0.73).

1. Introduction

The observed warming of the global climate is generally explained to have its most important cause in the cumulative emissions of carbon dioxide (CO₂) as a consequence of human industry, by burning fossil fuels or by producing cement. The available observation data was analysed to ascertain if the effect of CO₂ can be disentangled from other causes in a statistically significant way. The absorption of electromagnetic radiation by so-called greenhouse gases in the infrared range is a proven phenomenon that results in the radiative forcing of the atmosphere, accompanied by a rise of the global temperature. The magnitude of such rise depends on the gas concentrations, on their absorption factors, and on the feedbacks that the climate system gives to the primary radiative forcing. To ascertain the impact of human cause in climate change it is of utmost importance to quantify the overall temperature sensitivity to greenhouse gas concentration, in particular CO₂. This was made by comparing model calculation results with experimental regression formula derived from the available datasets.

¹ MR-int Michel de Rougemont Enterprise consulting, Kaiseraugst, Switzerland,
michel.de.rougemont@mr-int.ch

2. Actual observations

Available monthly data series from publicly accessible internet sites were retrieved:

Ta: Global surface temperature anomalies since 1850, HADCRUT4 (1)

CO₂: Carbon dioxide atmospheric concentration, since 1749, annual until 1959 (2)

AMO: Atlantic Multidecadal Oscillations, since 1856 (3)

SSN: Solar Spot Numbers, since 1750 (4)

TSI: Total Solar Irradiance since 1978, very similar to SSN (5)

SRT: Solar Radiation Transmittance, since 1958 (6)

MEI: Multi variate ENSO Index (El Niño - La Niña), since 1950 (7)

GSL: Global Sea Level since 1807 (8)

Data handling.

Centred running averages were calculated in order to eliminate short term variations that have no implications on long term climate change.

Over a 7 years period: Ta, CO₂, AMO, MEI and GSL,

Over a 13 months period: SSN

Not smoothed: SRT

Not used: TSI because its frequency coincides with that of SSN, available since 1750.

The Rate of Change (RoC), or volatility, the velocity at which a parameter changes over time, is also calculated over a 7 year centred running period for Ta (expressed in °C per century), CO₂ (in ppm per year), and GSL (in mm per year).

Other, non-global observation:

MFD: Magnetic Field Declination (9).

No average value can be validly calculated from a grid over the globe, as it is done for temperature anomalies. A representative evaluation is used by applying the model calculation to one single, randomly chosen place: Neuchâtel, Switzerland,
Elevation: 0.533 km Mean Sea Level, Latitude: 47.000, Longitude: 6.920 degrees.

These time series are shown on Figure 1.

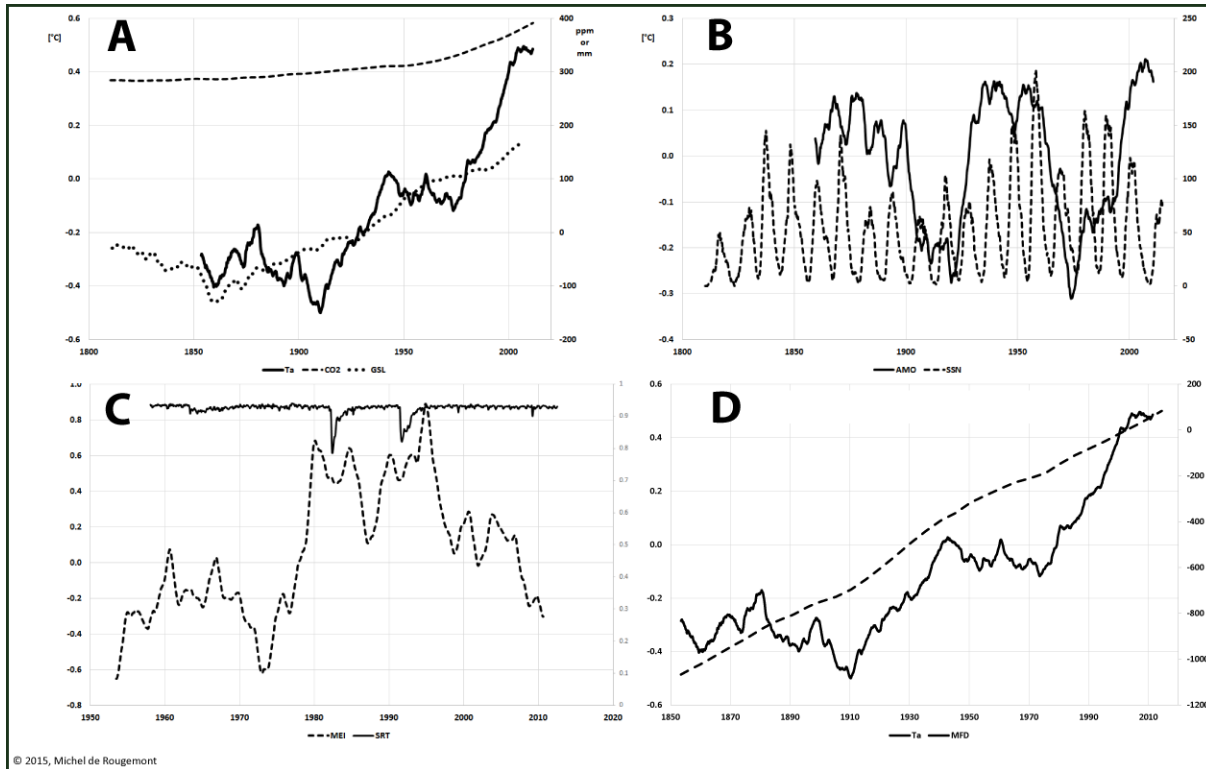


Figure 1 Available observed parameters. Smoothed and centred over 7 years (except SSN).
A: The principal dimensions
 Temperature anomalies T_a , reference 1961-1990, solid line, left scale
 CO₂ atmospheric concentration, broken line, right scale
 Global sea level GSL , dotted line, right scale
B: Oscillations
 Atlantic multidecadal oscillations AMO , solid line, left scale
 Solar spot Number SSN , dotted line, smoothed and centred over 13 months, right scale
C: Newest parameters, since the 1950s
 Multi-variate ENSO index MEI , dotted line, left scale
 Solar radiation transmittance SRT , solid line, right scale.
D: Temperature anomalies, as in A
 Magnetic Field Declination angle, dotted line, right scale

3. Correlations

Rates of Change of T_a , GSL , CO_2 , and MFD are represented on Figure 2. They correlate with time with following coefficients:

		Linear Correlation coefficient r^2
RoC T_a	$d(T_a)/dt$	0.1332
RoC GSL	$d(GSL)/dt$	0.2412
RoC CO_2	$d(CO_2)/dt$	0.7267
RoC MFD	$d(MFD)/dt$	0.0171

Table 1 Linear, time dependence correlation coefficients

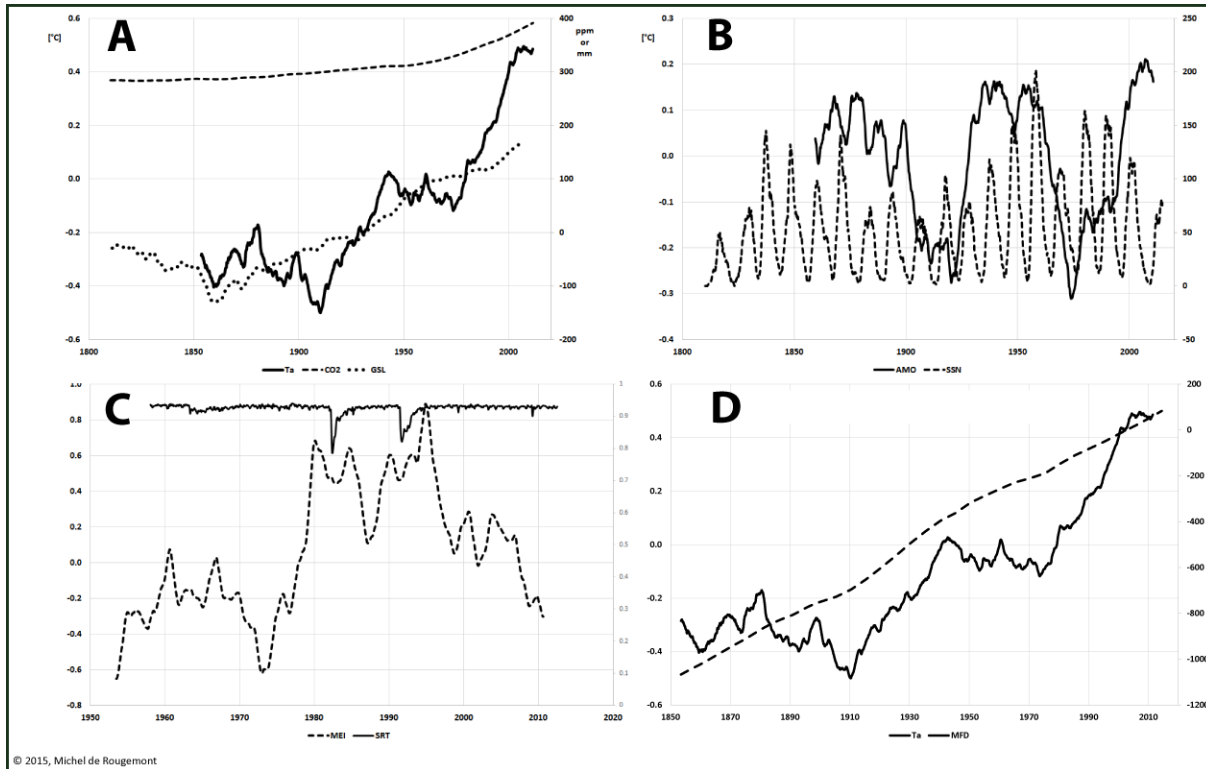


Figure 2 Rates of Change in function of the time.
 A: Temperature anomalies, RoC Ta, $d(Ta)/dt$, [$^{\circ}C$ per century]
 B: Global sea level RoC GSL, $d(GSL)/dt$ [mm/a]
 C: CO₂ concentration RoC CO₂, $d(CO_2)/dt$ [ppm/a]
 D: Magnetic Field Declination RoC MFD, $d(MFD)/dt$ [minutes/a]

A second correlation evaluation is made by using mutual dependencies among the three parameters, as shown on Figure 3:

Pearson correlation between	Coefficient ρ	Goodness of fit r^2
Ta and CO ₂	0.937645	0.879179
GSL and CO ₂	0.916315	0.839633
GSL and Ta	0.857879	0.735957
Ta and MFD	0.873845	0.763605

Table 2 Pearson correlation coefficient on mutual dependencies among Ta, CO₂, GSL, and MFD.

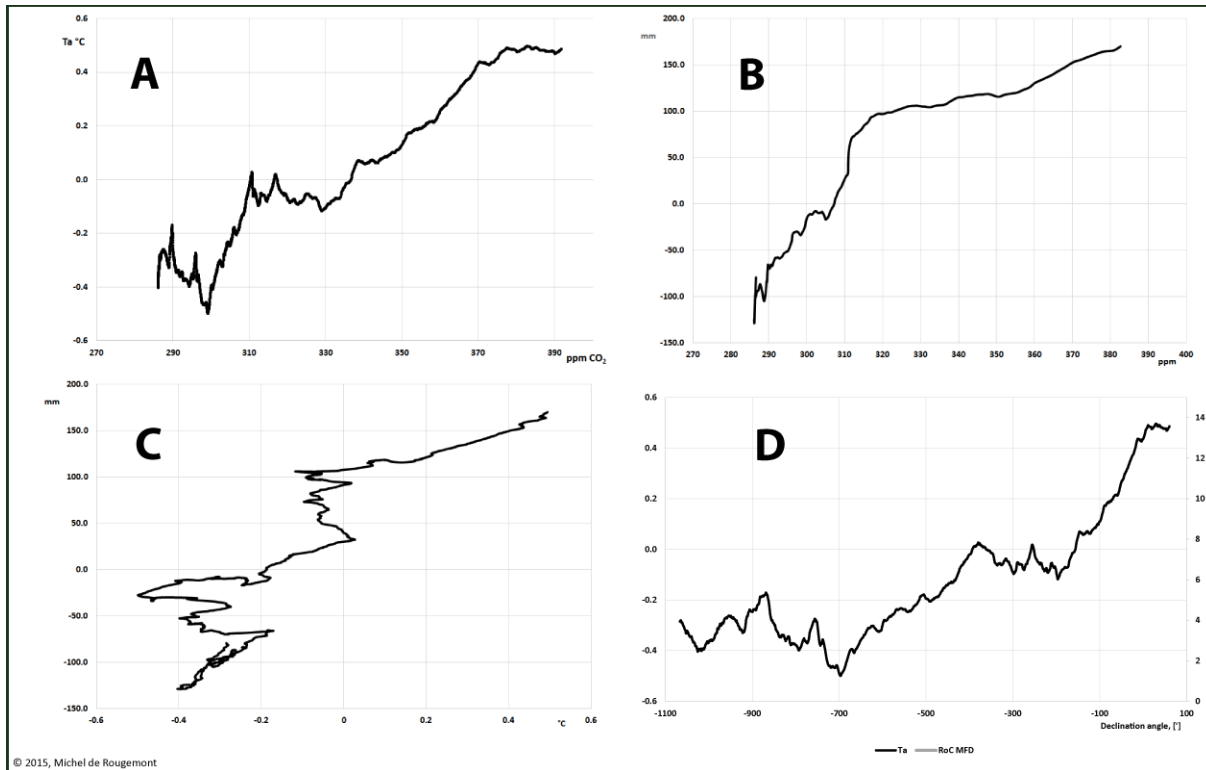


Figure 3 Mutual dependencies between temperature anomalies (TA), CO₂ concentration, and global sea level (GSL)

A: $Ta = f(CO_2)$

B: $GSL = f(CO_2)$

C: $GSL = f(Ta)$

D: $Ta = f(MFD)$

A third correlation evaluation is also made using the rates of change of the three parameters shown on Figure 4.

Pearson correlation between	Coefficient ρ	Goodness of fit r^2
RoC Ta and CO ₂	0.407734	0.166247
RoC GSL and CO ₂	0.037299	0.001391
RoC GSL and Ta	0.104207	0.010859
RoC Ta and MFD	0.294620	0.086801

Table 3 Pearson mutual correlation of the rates of change of temperature anomalies (Ta) and global sea level (GSL) with CO₂, between them, and with MFD.

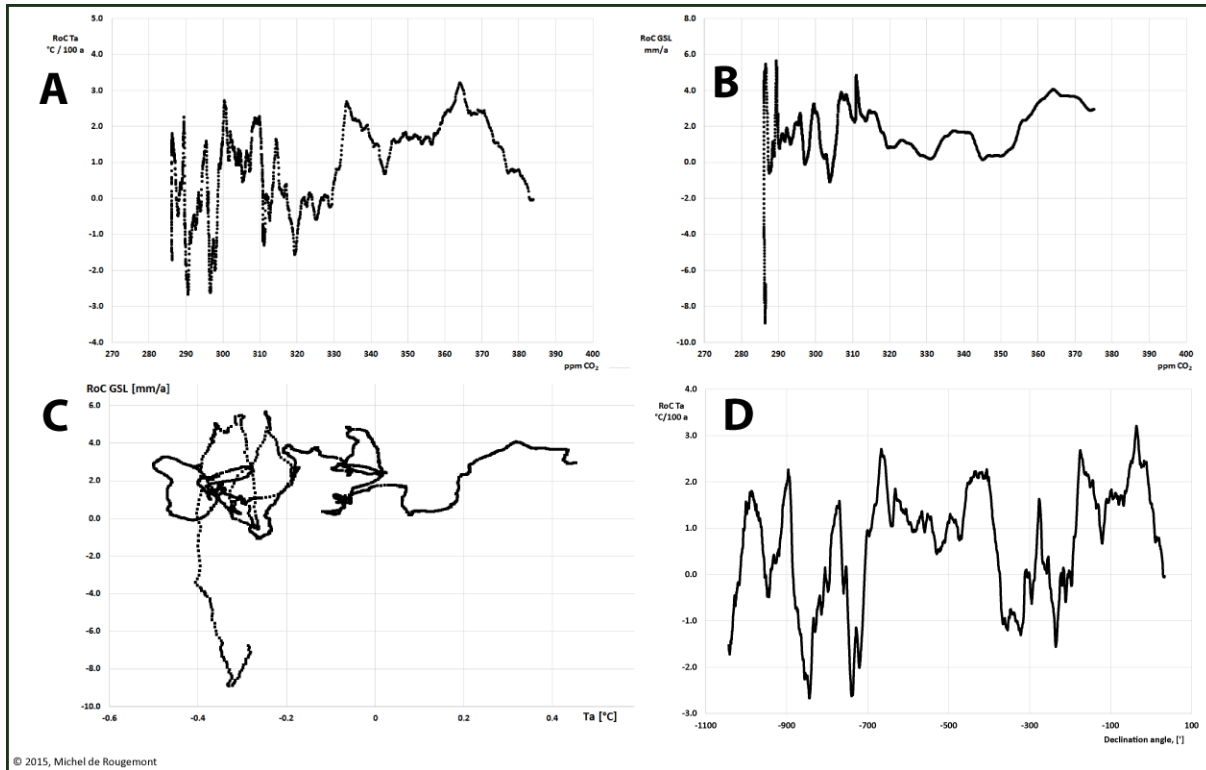


Figure 4 Rates of change as function of CO2 concentration and of temperature anomalies

A: $RoC Ta = f(CO_2)$

B: $RoC GSL = f(CO_2)$

C: $RoC GSL = f(Ta)$

D: $RoC Ta = f(MFD)$

4. Regression analysis

A multivariate regression calculation is made using all available data series. The software Eurequa-Pro-trial was used to this effect (10).

For the older data series a regression formula was found expressing Ta as a function of AMO, CO2, GSL, and SSN:

$$\text{Formula 1: } Ta = 0.455945 * AMO + 0.00864923 * \text{delay}(CO_2, 32) + .000997215 * GSL + .00175582 * GSL * AMO * \cos(0.106703 * \text{delay}(GSL, 34)) - 2.82996 - 7.45672e-6 * \text{delay}(GSL, 34)^2 - 0.3619303 * AMO * \cos(0.106703 * \text{delay}(GSL, 34))$$

r^2 goodness of fit = 0.9934

SSN, the solar spot number, was not retained as a significant parameter.

The delays are given in months

For the more recent period, the parameters SRT and MEI were added to the dataset. The following regression formula was found:

$$\text{Formula 2: } T_a = 1.04651 + 0.217831 * \text{AMO} + 0.0355494 * \text{delay}(\text{MEI}, 2) + 0.00352686 * \text{GSL} + 0.000183110 * \text{SSN} + -465.364 / \text{CO}_2 - 0.0363844 * \cos(0.0753817 * \text{CO}_2 + \text{delay}(\text{AMO}, 10) + \text{delay}(\text{MEI}, 89))$$

$$r^2 \text{ goodness of fit} = 0.9991$$

SRT, the solar radiation transmission, was not retained as a significant parameter

The same regression analysis can be made to evaluate a formula that includes magnetic field declination angle (MFD), $T_a = f(\text{CO}_2, \text{GSL}, \text{Spots}, \text{AMO}, \text{MFD})$:

$$\text{Formula 3: } T_a = 0.419630 * \text{AMO} + 0.419630 * \text{delay}(\text{CO}_2, 2) + 0.000280069 * \text{delay}(\text{MFD}, 95) + 0.000713600 * \text{delay}(\text{AMO}, 14) * \text{delay}(\text{MFD}, 95) * \cos(0.5972651 * \text{CO}_2 + \cos(\text{AMO} + 0.419630 * \text{delay}(\text{CO}_2, 2))) - 2.461346 - 0.411643 * \text{CO}_2 - 0.419630 * \text{delay}(\text{AMO}, 14)^2 * \cos(0.597265 * \text{CO}_2 + \cos(\text{AMO} + 0.419630 * \text{delay}(\text{CO}_2, 2)))$$

$$r^2 \text{ goodness of fit} = 0.9958$$

Also, when excluding CO_2 , a regression formula is obtained for $T_a = f(\text{GSL}, \text{Spots}, \text{AMO}, \text{MFD})$.

$$\text{Formula 4: } T_a = 0.515185 + (\text{AMO} * \text{MFD} + 4.459986 * \text{AMO} * \text{delay}(\text{MFD}, 57) * \text{delay}(\text{AMO}, 126) - 1.049517 * \text{MFD}) / \text{delay}(\text{MFD}, 329) + (78.76953 * \text{AMO} + 413.4848 * \text{AMO} * \text{delay}(\text{AMO}, 126)) / (0.5151853 * \text{delay}(\text{MFD}, 329) - \text{delay}(\text{AMO}, 146) * \text{delay}(\text{MFD}, 329))$$

$$r^2 \text{ goodness of fit} = 0.9916$$

An “observed temperature rise” can be evaluated by subtracting the oscillating components AMO, SSN, MEI from the full formula, as shown on Figure 5. In this case the two parameters having a ramping pattern over the period of observation, GSL and CO_2 , serve as proxies for all similarly behaving phenomena that may be in play during this same time.

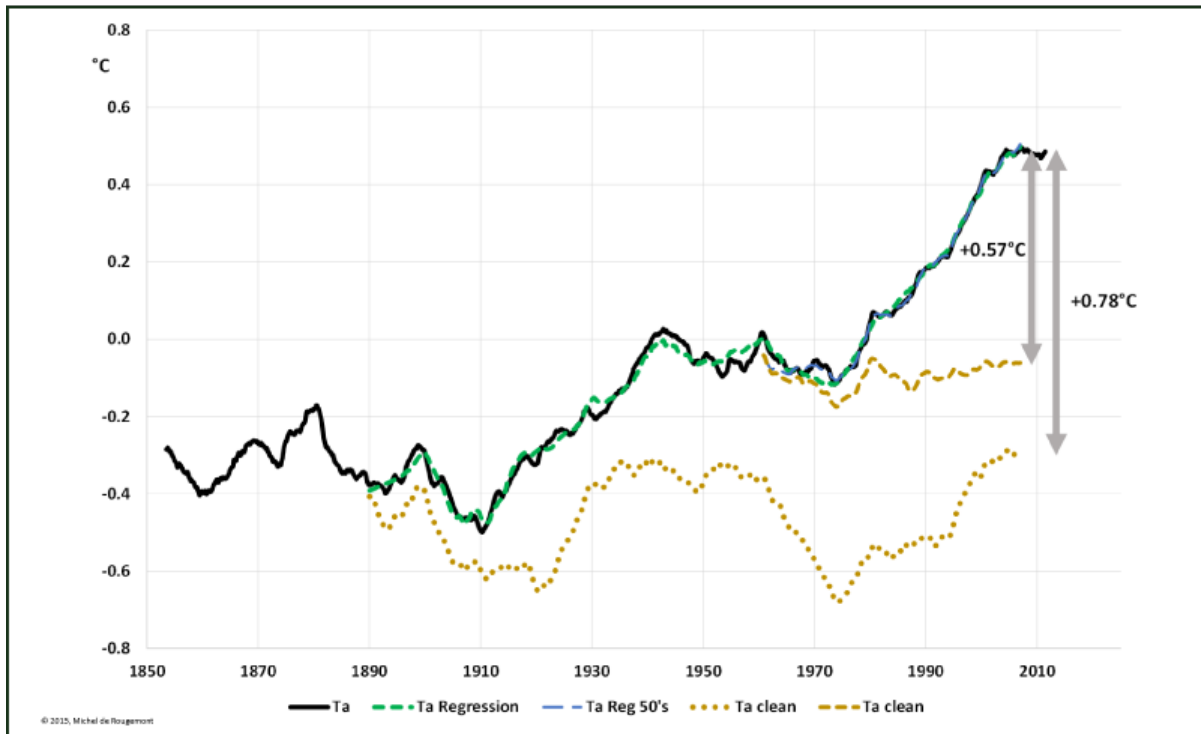


Figure 5 Regression lines for temperature anomalies as function of CO_2 , AMO, SSN, GSL, and MEI, using formula 1 for the long time period, and formula 2 for recent, more precise and complete data. The lines named “Ta clean” are computed by keeping constant CO_2 and GSL at the initial value of the corresponding calculation period.

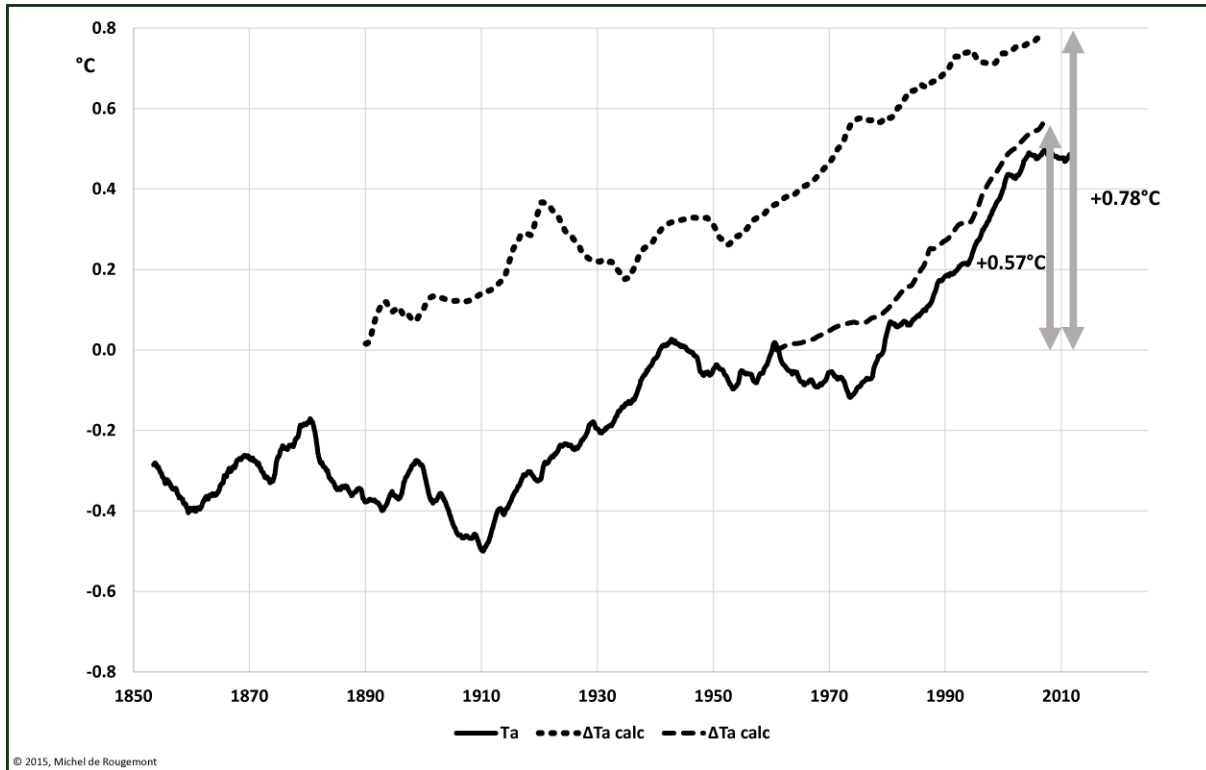


Figure 6 Temperature anomalies and calculated ΔT_a according to formula 1 and 2.

5. Equilibrium Climate Sensitivity

Radiative forcing results from the absorption of electromagnetic radiations in the infrared range by so-called greenhouse gases that are present in the atmosphere, among which CO_2 . As this primary radiative forcing is taking place, the Earth climate system responds by an elevation of the atmospheric temperature, and subsequently by a series of feedbacks.

The primary radiative forcing is approximated with the practical formula of Myhre (11):

$$F_{GHG} = \ln\left(\frac{C_1}{C_0}\right) \quad (\text{equation 1})$$

Where F_{GHG} = forcing [W m^{-2}]

C_0 and C_1 = initial and final CO_2 concentration [ppmV or mol%]

The temperature change resulting from a rise of the CO_2 concentration is calculated as

$$\Delta T = \frac{G_S}{(1 - G_S \cdot G_F)} \cdot F_{GHG} \quad (\text{equation 2})$$

Where

G_S = Primary system response = $\Delta T / F$ [$\text{K W}^{-1} \text{m}^2$]

G_F = System feedback response = $F / \Delta T$ [$\text{W m}^{-2} \text{K}^{-1}$]

Climate feedback factors are reviewed in the latest report (12) of the Intergovernmental Panel on Climate Change (IPCC).

The model calculation based on a feedback system is explained and developed in the appendix.

The anticipated temperature response from this model is compared with the observed rate of change of the temperature (RoC Ta) over the actual range of variation of the CO₂ concentration.

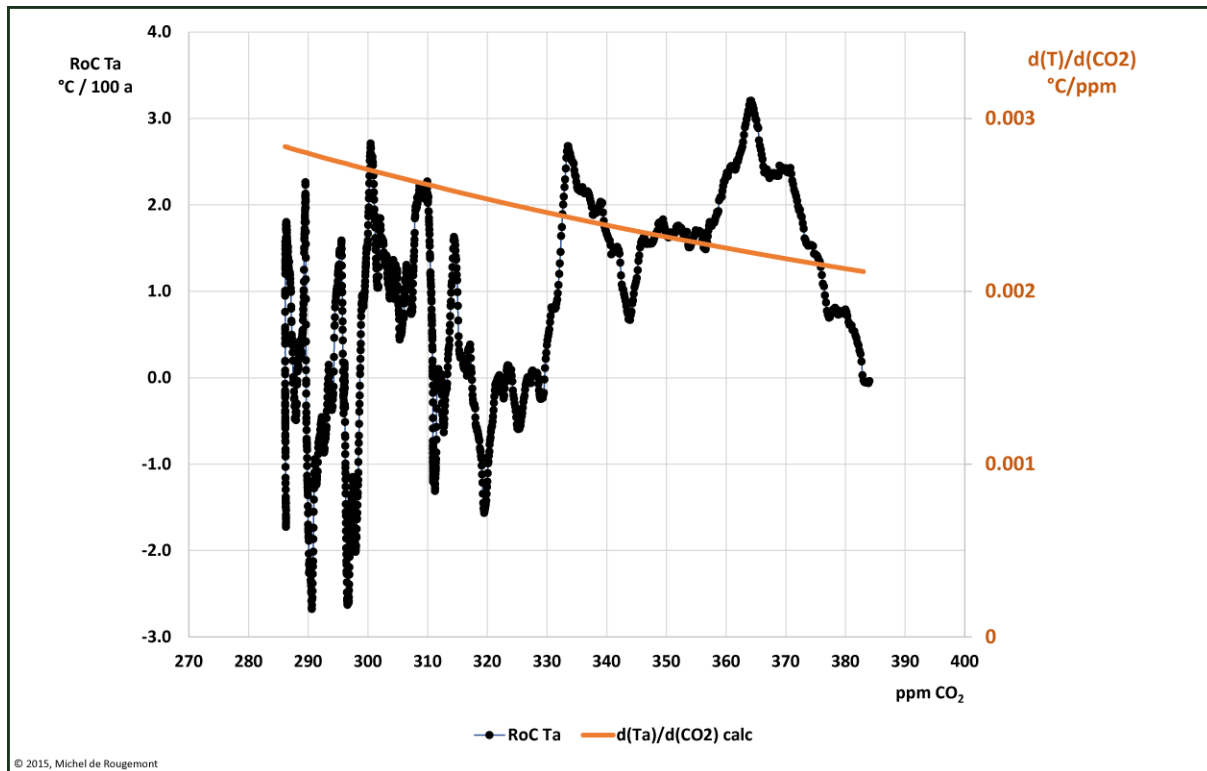


Figure 7 Rate of change of temperature anomalies (left scale) and expected temperature sensitivity to CO₂ (right scale) calculated with $GS = 0.187 \text{ K W}^{-1} \text{ m}^2$ and $GF = -1.59 \text{ W m}^{-2} \text{ K}^{-1}$

The Equilibrium Climate Sensitivity in the sense given to this expression by IPCC (temperature increase for a doubling of CO₂ concentration) was calculated as:

$$ECS = 0.53 \text{ }^\circ\text{C} \text{ (0.42 to 0.73)}$$

On Table 4 the observed temperature rises (ΔT) shown on Figure 6 are compared with values calculated by using the model.

	ΔT observed	CO ₂ concentration [ppm]		ΔT calculated	Potential CO ₂ contribution to warming.
		Beginning	End		
Since beginning of the industrial era (no smoothing)	1.05 °C	280	400	0.28 °C	27%
Using Formula 1	0.78 °C	293	383	0.21 °C	27%
Using Formula 2	0.57 °C	317	383	0.14 °C	25%

Table 4 Observed and calculated temperature rises.

The contribution of CO₂ is calculated using equations 1 and 2.

The useful observation period is narrowed by data smoothing with running averages over 7 year.

6. Discussion

The available experimental data provides from a relatively short period. It spans over 160 years, with a global warming of 1°C, 42% increase of CO₂ concentration, 300 mm sea level rise, and a shift of 19 degrees of the magnetic field declination. As can be seen on Figure 1, Ta, GSL, MFD, and CO₂ show a ramping, cumulative pattern over the observation period, while AMO, SSN, MEI are oscillating, and SRT shows only disturbances linked with volcanic eruptions.

The correlation coefficients in Table 1 indicate that the rate of change of the CO₂ concentration (RoC CO₂) may have a time dependent, historic development; the acceleration taking place since the end of the 1940's coincides with the strong worldwide economic development which started just after World War II.

Correlation coefficients of Table 2 indicate probable mutual correlations among Ta, GSL, MFD, and CO₂.

However, as shown in Figure 4 the rates of change of temperature (RoC Ta) or sea level (RoC GSL) are visibly volatile in relation with the CO₂ concentration; this is confirmed in Table 3 by the low probability of a correlative relationship of these rates of change as a function of the CO₂ concentration. The same lack of probability applies for RoC Ta in relation with MFD.

It follows from this correlation analysis that the observed warming cannot be related in a statistically significant way to one or the other parameters observed over the period for which data series are available. It is therefore certain that no mono-causal relationships associating global warming with CO₂ concentration, or with sea level, or with magnetic field can be established with the limited available experimental data. Thus, any contribution of one of these parameters can only be approximated by model evaluations based on plausible physical phenomena.

By multivariable regression analysis, cumulative, ramping up variables can be separated from the ones that oscillate at frequencies inducing temporary weather changes; a close fit between observed and calculated temperature anomalies is shown in Figure 6. Using the regression

formula 1 and 2, the calculated temperature increases ΔT_a shown in Figure 7 are separated from the effect of oscillating variables, of which multi-decadal oscillations such as AMO and MEI play a large part (similar evaluations made with unsmoothed data or with regression formula 3 and 4 lead to similar calculated ΔT_a).

In Figure 7 there is a marked contrast between the observed volatility of the temperature rate of change (RoC T_a) and the expected temperature response to CO_2 concentration according to a simple, plausible, and easily verifiable model calculation that encompasses radiative forcing together with estimated feedback factors. The calculated CO_2 contribution to the observed global warming may have been of the order of 25 to 30% of the total, as shown on Table 4. In such calculation, the most important parameters are the 5.35 coefficient in equation 1, and the overall stabilizing feedback factor G_F that is derived from already complex models. In its 1990 report, IPCC used a factor 6.3 in equation 1. The correction made by Myhre in 1998 has been re-assessed in a recent study by Reinhart (13), obtaining a value of 1.88, roughly one third of Myhres's estimate. Thus the CO_2 contribution to warming could be even one third of the one calculated in Table 4, or less than 10% of the global warming. To attribute the whole observed warming to the sole CO_2 concentration increase would require a correction of the feedback factor G_F from a stabilizing negative value of -1.59 to a positive one of +3.5 $\text{K W}^{-1} \text{ m}^2$, implicating a high instability of the whole climate system, contrary to observations made after volcanic eruptions and to other history climate evolutions, as well as to all climate feedbacks reviewed by IPCC.

Furthermore, IPCC affirms in its Technical Summary (14): "Estimates of the equilibrium climate sensitivity (ECS) based on observed climate change, climate models and feedback analysis, as well as paleoclimate evidence indicate that ECS is positive, *likely* in the range 1.5°C to 4.5°C with *high confidence*, *extremely unlikely* less than 1°C (high confidence) and *very unlikely* greater than 6°C (*medium confidence*)".

Demonstrating that no correlation is identifiable with available observed data, and calculating ECS at 0.53°C (0.42 to 0.73) in a simple and verifiable way, the present study cannot confirm such categorical and oracular statement. The common belief of a preponderant human influence on climate change by CO_2 emissions has therefore not enough validity to justify the proposed goals and programmes for drastic global emission reductions.

Other so-called greenhouse gases as well as so far not identified or quantified phenomena must be in play to make up for the remaining 70-75%, or even 90%, of the global warming. The facts that glaciers began their melting and seas their rising well before the beginning of the industrial era confirm the plausibility of that affirmation, although no satisfying explanations or quantitation are yet available to demonstrate it.

In view of the limited availability of observation data and of the fact that no other experimental work can be performed beyond monitoring the actual climate evolution, it can be expected that for an extremely long time, centuries, no better disentanglement of possible causes will allow to construct reliable and valid climate theories.

Appendix.

Calculated climate sensitivity

Radiative forcing resulting from the absorption of electromagnetic radiations in the infrared range is approximated with the practical formula of Myhre (11):

$$F_{GHG} = \ln\left(\frac{C_1}{C_0}\right) \quad (\text{equation 1})$$

Where F = forcing [W m^{-2}]

C_0 and C_1 = initial and final CO_2 concentration [ppmV or mol%]

Thus, according to Myhre, if the CO_2 concentration doubles: $F = 3.71 \text{ W m}^{-2}$.

As primary radiative forcing is taking place, the system responds by an elevation of the atmospheric temperature, and subsequently by a series of feedbacks. At the equilibrium the system can be described by a block diagram.

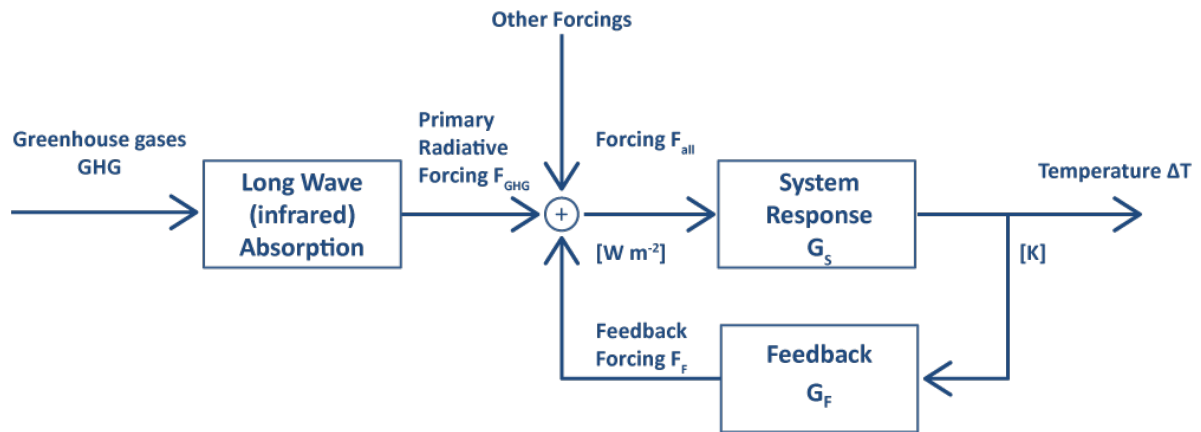


Figure 8 Simplified block diagram of climate response to radiative forcing caused by a greenhouse gas.

F_{GHG} = Forcing resulting from the absorption of long wave radiations by greenhouse gases

F_F = Forcing resulting from feedback mechanisms [W m^{-2}]

$F_{all} = F_{GHG} + F_F$

ΔT = Surface temperature variation resulting from the total forcing [K]

G_S = Primary system response = $\Delta T / F_{all}$ [$\text{K W}^{-1} \text{ m}^2$]

G_F = System feedback response = $F_F / \Delta T$ [$\text{W m}^{-2} \text{ K}^{-1}$]

Applying the transfer functions G_S and G_F , and resolving for ΔT :

$$\Delta T = G_S \cdot F_{all}$$

$$F_F = G_F \cdot \Delta T$$

$$F_{\text{all}} = F_{\text{GHG}} + F_{\text{F}} = F_{\text{GHG}} + G_{\text{F}} \cdot \Delta T$$

$$\Delta T / G_{\text{S}} = F_{\text{GHG}} + G_{\text{F}} \cdot \Delta T$$

$$\Delta T \cdot (1 - G_{\text{F}} \cdot G_{\text{S}}) = G_{\text{S}} \cdot F_{\text{GHG}}$$

$$\Delta T = \frac{G_{\text{S}}}{(1 - G_{\text{S}} \cdot G_{\text{F}})} \cdot F_{\text{GHG}} \quad (\text{equation 2})$$

The primary transfer function of the system is given by the derivative of the Stefan Boltzman equation:

$$F = \varepsilon \cdot \sigma \cdot T^4 \quad \text{or} \quad T = (F / (\varepsilon \cdot \sigma))^{0.25} \quad \text{thus:}$$

$$G_{\text{S}} = \frac{dT}{dF} = \frac{1}{4 \cdot \varepsilon \cdot \sigma} \cdot \left(\frac{F}{\varepsilon \cdot \sigma} \right)^{-\left(\frac{3}{4}\right)} \quad (\text{equation 3})$$

This derivative is dependent of the radiation intensity which at its turns is a function of temperature, as seen on Figure 2, calculated with $\varepsilon = 1$.

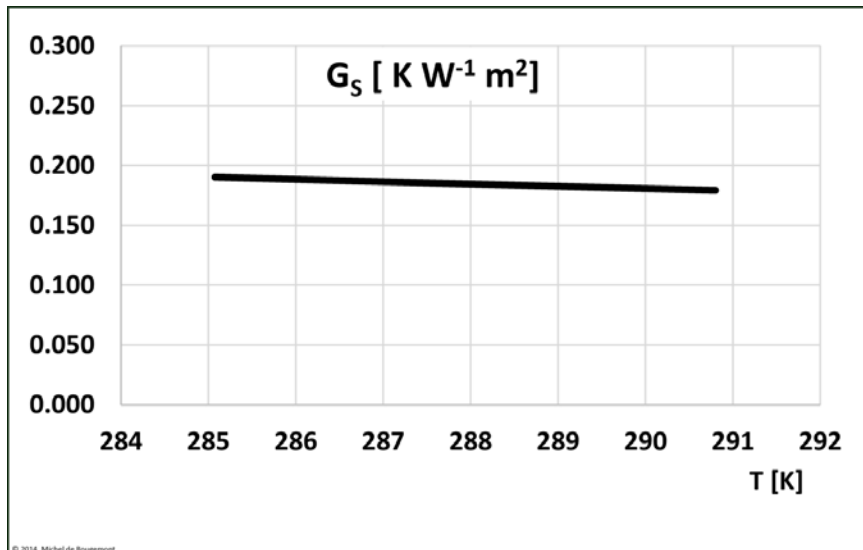


Figure 9 Transfer function G_{S} at Earth surface temperature

To simplify, around 286-289 K, the average Earth surface temperature, this transfer function can be linearized at:

$$G_{\text{S}} = 0.187 \text{ K W}^{-1} \text{ m}^2.$$

The feedback transfer function G_F is taken as the sum of the average individual values summarized on table 9.5 of the 5th IPCC report (12). The associated phenomena are:

Planck: As temperature increases, the radiative energy emitted will also increase according to Planck law. While losing this energy, the temperature of the emitting material will decrease. Part of the temperature increase contributes therefore to eliminate the forcing, and to dampen the temperature rise. Thus, Planck response is a negative feedback:

$$\lambda_P = -3.21 \pm 0.11 \text{ W m}^{-2} \text{ K}^{-1}$$

Water Vapour: More water will evaporate when temperature is increasing. The higher air humidity will absorb more radiative energy and contribute to amplifying the forcing. This is a positive feedback:

$$\lambda_{WV} = 1.63 \pm 0.33 \text{ W m}^{-2} \text{ K}^{-1}$$

However, the evaporation-condensation of water, with its large latent heat (2444 J g⁻¹ at surface temperature), is not considered in this parameter. Another model would be required to reflect this.

Lapse Rate: The lapse rate is the temperature gradient that establishes itself from the surface up to the top of the mesosphere. When the overall temperature increases, the structure of the atmosphere will change, convective force will move warmer air upwards and the gradient will change: it will tend to be less pronounced in tropical latitudes (negative feedback) and more pronounced in mid-latitudes (positive feedback). Overall it results to be a negative feedback, with a large uncertainty:

$$\lambda_{LR} = -0.60 \pm 0.46 \text{ W m}^{-2} \text{ K}^{-1}$$

Albedo: The reflectivity of the sunlight depends on the type and on the extent of the surface that is reflecting it. In particular there is a large difference between ice and water. With higher temperature, less ice or snow coverage is expected, resulting in less reflection. This is a positive feedback:

$$\lambda_A = 0.31 \pm 0.11 \text{ W m}^{-2} \text{ K}^{-1}$$

Clouds: Clouds show two different feedbacks. With higher temperature, water will evaporate and more clouds will be formed. With a larger reflective surface, cloud albedo will increase, more sunlight will be reflected back to the outer space, a negative feedback. But at higher altitude the clouds will contribute to more radiative forcing in the IR range. Overall the current estimate is that it is a positive feedback, albeit with a high uncertainty (300%):

$$\lambda_C = 0.28 \pm 0.84 \text{ W m}^{-2} \text{ K}^{-1}$$

Overall, these factors are additive, resulting in a negative feedback:

$$\lambda = \lambda_P + \lambda_{WV} + \lambda_{LR} + \lambda_A + \lambda_C = -3.21 + 1.63 - 0.60 + 0.31 + 0.28 = -1.59$$

and by adding the error ranges:

$$G_F = \lambda = -1.59 [\pm 1.85] \text{ W m}^{-2} \text{ K}^{-1}$$

The overall negative value of G_F feedback indicates a dampening of the system in response to the primary radiative forcing.

The calculated ΔT in relation with CO_2 concentration is shown in Figure 10:

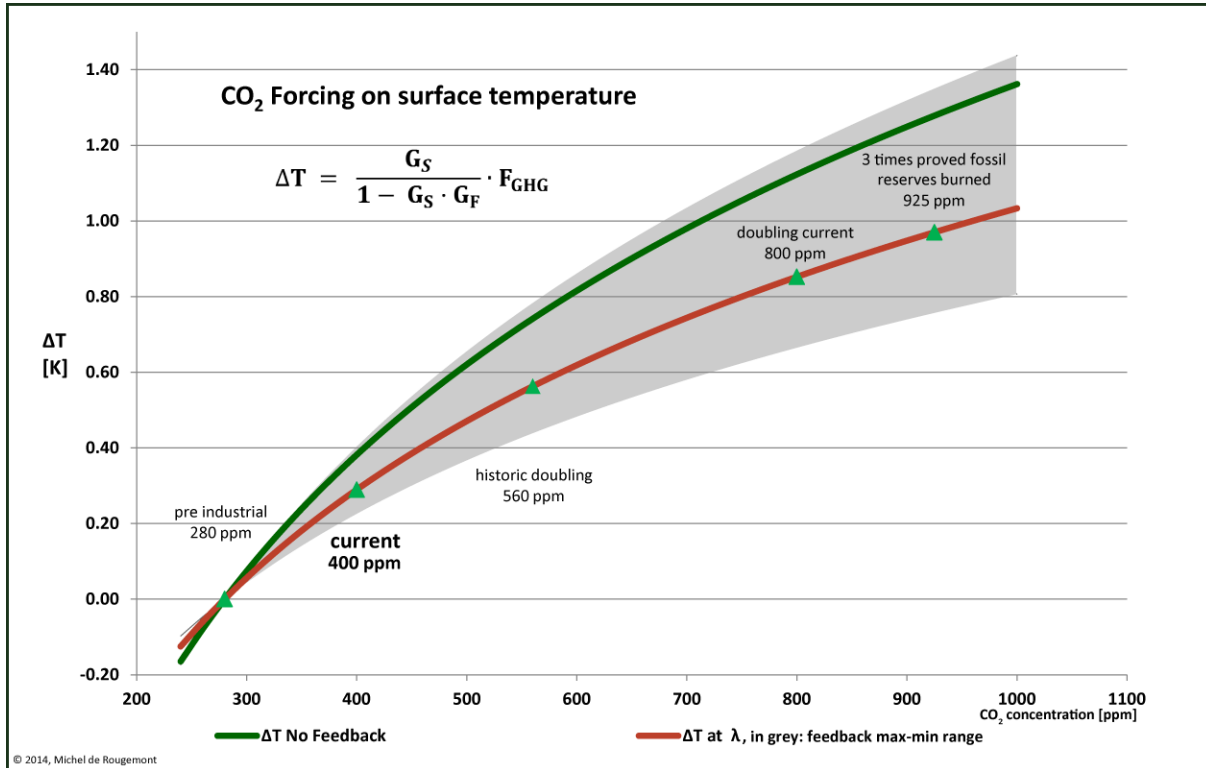


Figure 10 Calculated temperature sensitivity to CO_2 .

The grey area indicates the range of uncertainty of the feedback factor G_F .

Thus Equilibrium Climate Sensitivity in the sense given to this expression by IPCC (temperature increase resulting from doubling of the CO_2 concentration) is calculated as:

$$ECS = 0.53 \text{ K} \quad (0.42 \text{ to } 0.73)$$

Extrapolated to a hypothetical burning of 3 times the proved fossil reserves (15), with the CO_2 concentration reaching approximately 925 ppm, would imply:

$$\Delta T = 0.92 \text{ K} \quad (0.73 \text{ to } 1.26), \text{ since the beginning of the industrial era.}$$

References

- (1) Ta: Global surface temperature anomalies since 1850, Hadley Climate Research Center <http://www.metoffice.gov.uk>
HadCRUT4: monthly median near surface temperature data
temperature anomalies (°C) relative to 1961-1990.
- (2) CO₂: Carbon dioxide atmospheric concentration, since 1749, annual until 1959
Law Dome Ice Core yearly (before 1958)
http://www.ncdc.noaa.gov/paleo/icecore/antarctica/law/law_data.html
MacFarling Meure et al. (2006) 2000-Year CO₂, CH₄, and N₂O Data, after 1958: monthly average Mauna Loa observatory
<http://www.esrl.noaa.gov/gmd/ccgg/trends/>
- (3) AMO: Atlantic Multidecadal Oscillations, since 1856 (5)
Atlantic Multidecadal Oscillation,
<http://www.esrl.noaa.gov/psd/data/timeseries/AMO>
<http://www.esrl.noaa.gov/psd/data/correlation/amon.sm.long.data>
- (4) SSN: Solar Spot Numbers,
WDC-SILSO, Royal Observatory of Belgium, Brussels, <http://sidc.be/silso/home>
- (5) TSI: Total Solar Irradiance since 1978, very similar to SSN
Physikalisch-Meteorologisches Observatorium Davos, www.pmodwrc.ch
- (6) SRT: Solar Radiation Transmittance, since 1958
<http://www.esrl.noaa.gov/gmd/grad/mloapt.html>
- (7) MEI: Multi variate ENSO Index (El Niño - La Niña), since 1950
<http://www.esrl.noaa.gov/psd/data/correlation/mei.data>
- (8) GSL: Global Seal Level, since 1807
Jevrejeva, S. , J.C. Moore, A. Grinsted, A.P. Matthews, G. Spada. 2014.
<http://www.psmsl.org/products/reconstructions/gslGPChange2014.txt>
Trends and acceleration in global and regional sea levels since 1807,
Global and Planetary Change, vol 113, 10.1016/j.gloplacha.2013.12.004

- (9) Magnetic Field Components
Magnetic Model: IGRF11 (calculator version)
<http://www.ngdc.noaa.gov/geomag-web/#igrfwmm>
- (10) Eureka-Pro trial, available at www.nutonian.com
- (11) Myhre et al.
New estimates of radiative forcing due to well mixed greenhouse gases.
Geophysical Research Letters, Vol. 25, No.14, pages 2715-2718, July 15, 1998
http://folk.uio.no/gunnarmy/paper/myhre_grl98.pdf
- (12) IPCC, 2013: *Climate Change 2013: The Physical Science Basis. Contribution of Working Group I to the Fifth Assessment Report of the Intergovernmental Panel on Climate Change* Stocker, T.F., D. Qin, G.-K. Plattner, M. Tignor, S.K. Allen, J. Boschung, A. Nauels, Y. Xia, V. Bex and P.M. Midgley (eds.). Cambridge University Press, Cambridge, United Kingdom and New York, NY, USA, 1535 pp.
Feedback factors are summarized on Table 9-5, page 818.
- (13) F. K. Reinhart, www.eike-klima-energie.eu/uploads/media/Infrared_absorption_capability_of_atmospheric_carbon_dioxide.pdf.
- (14) IPCC, *ibid.*, page 81
- (15) BP Statistical Review of World Energy, June 2014, <http://bp.com/statisticalreview>

List of Tables

Table 1	Linear, time dependence correlation coefficients
Table 2	Pearson correlation coefficient on mutual dependencies among Ta, CO ₂ , GSL, and MFD.
Table 3	Pearson mutual correlation of the rates of change of temperature anomalies (Ta) and global sea level (GSL) with CO ₂ , between them, and with MFD.
Table 4	Observed and calculated temperature rises.

List of Figures

Figure 1	Available observed parameters.
Figure 2	Rates of Change in function of the time.
Figure 3	Mutual dependencies between temperature anomalies (TA), CO ₂ concentration, and global sea level (GSL)
Figure 4	Rates of change as function of CO ₂ concentration and of temperature anomalies
Figure 5	Regression lines for temperature anomalies
Figure 6	Temperature anomalies and calculated ΔT_a according to formula 1 and 2.
Figure 7	Rate of change of temperature anomalies and expected temperature sensitivity to CO ₂
Figure 8	Simplified block diagram of climate response to radiative forcing
Figure 9	Transfer function G_s at Earth surface temperature
Figure 10	Calculated temperature sensitivity to CO ₂ .

Conflict of interest: Michel de Rougemont has no conflict of interest.

Financial support: none